ЖУРНАЛ ФІЗИЧНИХ ДОСЛІДЖЕНЬ
т. 16, № 1/2 (2012) 1903(11 с.)

JOURNAL OF PHYSICAL STUDIES
v. 16, No. 1/2 (2012) 1903(11 p.)

NON-LTE FORMATION OF THE SI I 1082.7 nm LINE IN ONE- AND THREE-DIMENSIONAL MODELS OF THE SOLAR ATMOSPHERE

A. V. Sukhorukov
Main Astronomical Observatory, NAS of Ukraine,
27, Acad. Zabolotnoho St., Kyiv, UA–03680, Ukraine,
e-mail: suh@mao.kiev.ua

(Received July 03, 2012; received in final form July 25, 2012)

The formation of the Si I 1082.7 nm line in several one-dimensional (1D) semi-empirical models and a three-dimensional hydrodynamical (3D HD) model of the solar atmosphere were studied. Significant departures from LTE were found in all the models. These departures are due to the line formation height shift and the line source function deficit. In the 3D model, the non-LTE line core intensity is much lower than those in the 1D models, if inelastic collisions with hydrogen atoms are neglected. In the 3D model a good agreement with observations can be obtained if the Drawin formula with a scaling factor $S_{\rm H} = 0.1$ is used to describe such collisions in order to compensate for strong non-LTE effects. In the 1D models, which do not describe the effects of real atmospheric ihnomogeneities, the best-fit is obtained with a higher value $S_{\rm H} = 1$. The best-fit oscillator strength $\log gf$ was estimated for this line. It is about 0.27 in the 1D models, and 0.24 in the 3D model.

Key words: line: formation, line: profiles, radiative transfer, Sun: atmosphere, Sun: infrared.

PACS number(s): 95.30.Jx, 95.30.Ky, 96.60.Mz

I. INTRODUCTION

One of the key problems of modern astrophysics is how stellar photospheres and chromospheres are dynamically coupled together, and what is the role of the magnetic field in this coupling. The identification of the chromospheric heating mechanisms is the most significant problem to be puzzled out in solar physics.

One of the ways to solve the problem is to carry out simultaneous observations of chromosphere and photosphere in the infrared (IR) spectral region near 1083 nm. This region contains a chromospheric triplet of He I 1083 nm and a photospheric line of Si I 1082.7 nm. The helium triplet is formed in the middle chromosphere at the heights around 2000 km. The silicon line is formed in the upper photosphere near 500 km, close to the temperature minimum. Our interest to the observations of these lines has been growing over the last fifteen years due to increased sensitivity of IR CCD devices, invention of fast polarization filters, and progress in the theoretical methods of polarized radiative transfer [1].

Both Si I 1082.7 and He I 1083 nm lines were used for multi-wavelength observations. Chuprakov et al. [2] observed the morphology and spectrum of a sunspot umbra in Si I, He I and H_α lines. Schad et al. [3] studied plasma flow along the magnetic field lines in a sunspot and nearby spiculae. For this purpose, an inversion of polarimetric observations of Si I, He I and Fe I 630 nm lines was made. Muglach et al. [4] applied a similar technique to the ground-based observations supported by SUMER observations in O I 115 nm and C III 117 nm lines, to investigate the dynamics of the quiet Sun atmosphere. Full-Stokes inversion was used to study active formations, such as sunspot umbra, penumbra and surrounding faculae [5, 6], chromospheric fibrils [7], active region filament [8, 9], complex active regions [10, 11], as well as eruptions [12].

In the Plan-B of the "Interim Report on the SOLAR-C Mission Concept" [13] the lines from the 1083 nm region are discussed as candidates for spectroscopic and polarimetric observations of the solar photosphere and chromosphere.

The Si I 1082.7 nm and the He I 1083 nm lines were used for studies of waves in the solar atmosphere. Centeno et al. [14] studied the propagation of shock waves from the photosphere to the chromosphere in a sunspot umbra, and the properties of such oscillations in a pore and a facula [15]. Felipe et al. [16–18] used observations of Si lines to simulate shock waves propagation in sunspots. In similar fashion, Hofmann et al. [19] measured phase relations of waves in different chromospheric structures. Bloomfield et al. [20, 21] observed the properties of running penumbral waves in a sunspot and surrounding regions of the quiet Sun. Penn & Allen [22] used magnetograms to compute the power of atmospheric wave oscillations near the north pole of the Sun. An overview of solar magnetic fields measurements with the 1083 nm region was made by Lagg [1]. Other applications of the Si I 1082.7 nm line in solar physics include: studies of long-term variations of solar activity [23] and measurements of solar differential rotation [24].

Both helium and silicon lines are formed out of local thermodynamical equilibrium (LTE). For correct interpretation of observations the non-LTE effects must be properly accounted for.

The most important non-LTE mechanism for He I triplet is caused by the coronal UV irradiation penetrating the chromosphere [25–27]. Moreover, this triplet is abnormally polarized and split in magnetic field via joint Hanle and Zeeman effects [28, 29].

The non-LTE line core intensity of the Si I 1082.7 nm line as well as the cores of the most solar Si I lines in the near-infrared solar spectrum are lower than the corresponding LTE values [30, 31].

Before the 2000s, such effects where not described in detail, because only visible lines of solar silicon spectrum were studied (mainly for abundance determinations). But during the last ten years, the infrared lines of Si I have been used in more comprehensive studies [32]. However, the observations of the Si I 1082.7 nm line are usually interpreted assuming LTE in 1D model atmospheres without the magnetic field. Milne–Eddington approximation is still used for the inversion of the Si I Stokes profiles.

Shi et al. [30] found considerable non-LTE effects in the cores of Si I lines with $\lambda > 1\,\mu$m. These authors showed that in order to reproduce the observed profiles, inelastic collisions with hydrogen atoms must be taken into account. They found an optimal scaling factor to the corresponding Drawin formula: $S_{\rm H} = 0.1$.

Bard & Carlsson [31] studied the formation of the Si I 1082.7 nm line in 1D models of a sunspot and a quiet solar atmosphere. Their main objective was to construct a computationally tractable atomic model of Si I, which is still able to reproduce the line profile in non-LTE with no significant change. The authors pointed out the non-LTE processes that affect the formation of this line. They did not include inelastic collisions with hydrogen atoms to avoid additional parameterization because there is no reliable atomic data for them, and such collisions may be important in metal-poor cool stars, not in the Sun. The discrepancy between computed and observed line core intensities was attributed in inability of 1D models to represent real atmospheric inhomogeneities. The authors assumed that the non-LTE line core will be less deep, if one considers convective velocities represented in a realistic 3D model.

In the last two articles discussed the non-LTE effects for the Si I spectrum are described only for 1D model atmospheres. So far, neither the line formation in realistic 3D model atmospheres, nor that in the presence of magnetic field in the model was considered.

Summarizing everything said above we formulate the following issues on the formation of the Si I 1082.7 nm line:

1. What is the difference between the non-LTE effects in this line in 1D and 3D model atmospheres?

2. What is the impact of atmospheric inhomogeneities (3D effects) on the line profile?

3. Is it possible to refine the line parameters such as an oscillator strength $\log gf$ and a scaling factor $S_{\rm H}$ for the Drawin formula using the non-LTE line simulations?

In this paper, we try to answer these questions.

II. METHOD

A. Atomic data and line parameters

We employed an atomic model of Si I and Si II described in our paper [33]. The model consists of 296 atomic energy levels including fine structure splitting, 4708 radiative transitions between them, and all corresponding non-radiative transitions.

Collisional excitation is of particular interest for our study. We used van Regemorter's formula for allowed transitions and Seaton's impact approximation for the rest of transitions with a parameterized value of the collisional strength Ω as it was described in our paper [33]. We varied Ω between 1 and 10 to test how inelastic collisions with electrons affect the resulting line intensity profile. Like Shi et al. and in contrast to Bard & Carlsson, we included inelastic collisions with hydrogen atoms using the Drawin formula [34, 35]. The scaling factor $S_{\rm H}$ for this formula was determined empirically by fitting computed to observed line profiles.

Line intensity profiles were computed for a selected set of oscillator strength values given in Table 1. We prefer the value $\log gf = 0.239$ of Froese-Fischer [40], which is recommended in the latest version of ASD NIST database [42].

$\log gf$	ref.	comment
0.10	[36]	f-sum rule
0.170	[36]	also in NIST v.3
0.191	[37]	LS-coupling without spin-orbital interaction
0.218	[38]	Scaled Thomas–Fermi method. Kurucz database [39] contains a similar value 0.22.
0.226	[37]	intermediate coupling with spin-orbital interaction
0.239	[40]	Breit–Pauli method, also in NIST v.4.1.0
0.273	[41]	LTE inversion. Rescaled from an original abundance value $A_{\rm Si} = 7.46$ to accepted in this work 7.55.

Table 1. Oscillator strengths of the Si I 1082.7 nm transition.

Van der Waals damping was calculated according to the theory of Anstee, Barklem, & O'Mara [43–46]. We computed the line profile in 1D models with the microturbulent velocity $V_{\rm mi}$ taken from the corresponding model. The macroturbulent velocity $V_{\rm ma}$ was derived from the formation height of the line following the recipe of Gurtovenko & Kostyk [47, p. 49]. For the 1D models used here this recipe gives $V_{\rm ma} = 1.85\,{\rm km\,s^{-1}}$. There is

no need for $V_{\rm mi}$ and $V_{\rm ma}$ parameters for the 3D model where they are substituted for the vector field of convective velocities. Here and below, the height of formation is defined according to the Eddington-Barbier approximation. It is the height where the optical depth at the line center is unity.

We used the solar silicon abundance $A_{\rm Si} = 7.55\,{\rm dex}$ recommended by Anders & Grevesse [48], which was a reference value before the 3D LTE abundance corrections were introduced by Asplund [50]. This value agrees with the recent non-LTE silicon abundance derived by Shchukina et al. [49].

B. Model atmospheres

Following our recent studies [33, 51] we used three 1D semi-empirical models of the quiet solar atmosphere: HOLMUL [52], MACKKL [53] and VAL-C [54]. These models have varied temperature distribution mainly in the upper atmospheric layers. In particular, there is no chromospheric rise in temperature in the HOLMUL model, while the VAL-C model is ∼200 K cooler in the temperature minimum than two other models. Hereinafter we denote the VAL-C as cool model, and two others as hot models. Such differences will clarify how the Si I 1082.7 nm line is sensitive to the temperature structure of the model atmosphere.

For our 3D calculations, a single 3D snapshot was taken from the radiative hydrodynamical simulations of solar surface convection [55, 57]. The dimensions of the domain are $6\times6\times3.8\,{\rm Mm}$ with $200\times200\times82$ grid points. It spans from the upper part of the convective zone to the lower chromosphere. We used only the uppermost 1 Mm layer for our radiative transfer computations. This layer was interpolated onto a coarser grid of $50\times50\times121$ points. Hereinafter this shapshot is called "3D model" for short.

In order to study spatial variations of the non-LTE effects in the 3D model we selected two 1D models corresponding to a granular and an intergranular lane. Following the classical definition our granule is an 1D model for which the continuum intensity is higher than the spatially-averaged continuum intensity in the 3D model. Accordingly, in the intergranule the continuum intensity is lower than the average value. We used a typical granule model with horizontal grid indices $X = 15$ and $Y = 5$, and a typical intergranule model with grid indices $X = 20$ and $Y = 5$.

The temperature distributions in our typical granule and intergranule differ from those of three semi-empirical models HOLMUL, MACKKL, and VAL-C (for illustration see Fig. 4 in [56]). First, in contrary to the models of MACKKL and VAL-C, there is no chromospheric rise in temperature both in the granular and intergranular models (as well as in the whole 3D model). Secondly, the granule has a higher temperature gradient than any semi-empirical model. The intergranule has lower temperature gradient than those three. Finally, deep layers of the granule are warmer than those in other models. The intergranule becomes warmer than the granule above 200 km. This effect is known as the granulation temperature inversion, and a similar effect holds for the velocity distribution [58, 59]. The temperature distribution in the granule is similar to those in the HOLMUL model above 200 km.

C. Computational method

The non-LTE calculations were performed with the NATAJA code developed by Shchukina & Trujillo Bueno [56]. The code solves the system of radiative transfer and statistical equilibrium equations for a given model atom in a 1D model atmosphere. It is based on a technique of accelerated Λ-iteration with preconditioning of rate equations and on a formal solver of radiative transfer equations using short characteristics method.

For the 3D model we neglected the effects of horizontal radiative transfer using the so-called 1.5D approximation. It means that the whole 3D domain was split into 2500 1D models. The system of radiative transfer and statistical equilibrium equations was solved independently for each model. The resulting profile of emergent intensity was spatially averaged over all 2500 models.

D. Comparison with observations

Two observed profiles were used for comparison: from the FTS atlas [60, 61], and from de Jager & Neven [62] (corrected for the instrumental profile). Both observations correspond to the solar disk center intensity.

III. RESULTS

A. Level populations

Figure 1(a, b) shows the population departure coefficients β for the lower $4s\,^3P^o_2$ ($E_l = 4.95\,{\rm eV}$) and upper $4p\,^3P_2$ ($E_u = 6.10\,{\rm eV}$) atomic levels of the Si I 1082.7 nm line. These coefficients are defined as $\beta \equiv n({\rm NLTE})/n({\rm LTE})$, where n denotes the population density of the corresponding atomic level in non-LTE or LTE, respectively. The results are shown for the models of HOLMUL and MACKKL to illustrate some differences due to different types of 1D models. The results for the VAL-C model are not shown because they are similar to those for the MACKKL model.

Such a behavior of the β coefficients results from the interaction of several non-LTE mechanisms described in detail in [33]. For the levels of the Si I 1082.7 nm transition the most important of them are the line scattering with photon losses, the photon suction, and the ultraviolet (UV) overionization.

The line scattering and photon losses manifest themselves as a divergence of the lower $4s\,^3P^o_2$ and upper $4p\,^3P_2$

levels of this line. Such a divergence results from the surface losses near the layer where the optical depth is unity. The losses propagate by scattering to far below that layer. The photon suction mechanism produces the slight excess of Si I atoms at the lower level in the photospheric layers below 600 km. The UV overionization depopulates both the lower and upper levels being stronger for the upper one. This overionization is caused by the UV radiation in continuum, which comes from the lower part of the atmosphere.

Figure 1(a, b) shows that, in general, the population of the lower level is close to LTE in the photosphere. In the uppermost layers of the model without chromosphere like the HOLMUL β_l of the lower level becomes less than unity, while in the model with chromosphere like the MACKKL $\beta_l > 1$. Such a behaviour of the β_l coefficient corresponds to the temperature stratification of the model atmospheres.

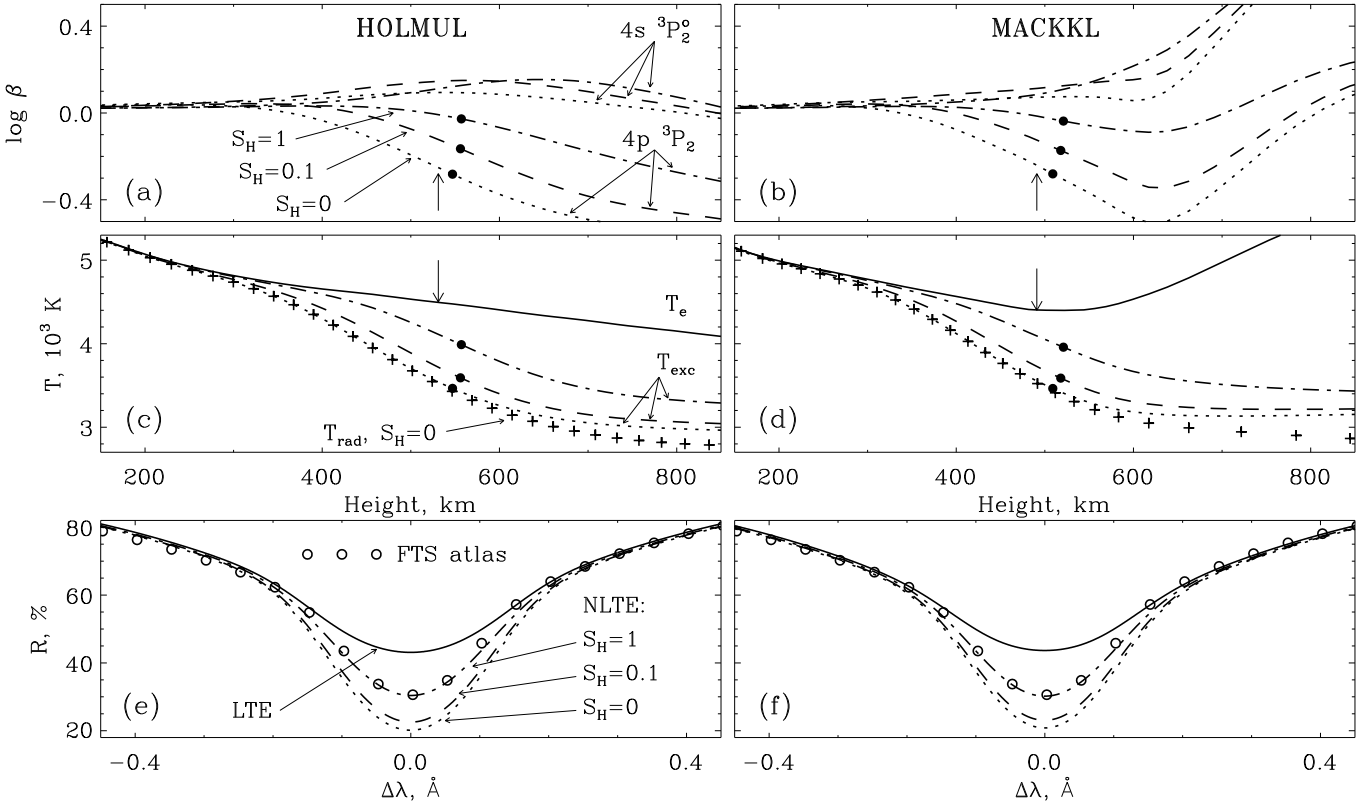

Fig. 1. Formation of the Si I 1082.7 nm line in the 1D models HOLMUL *(left panels)* and MACKKL *(right panels)* under LTE and non-LTE conditions. *Upper panels:* non-LTE departure coefficients β for the two levels of the line transition. *Middle panels:* the local electronic temperature T_e of the model which defines the local Plank function $B_\lambda(T_e)$; the excitation temperature T_{exc} and the radiation temperature T_{rad} defined by $S^L_\lambda = B_\lambda(T_{exc})$ and $\bar{J}_\lambda = B_\lambda(T_{rad})$, respectively, where S^L_λ is the line source function, and $\bar{J}_\lambda$ is the mean intensity in the line center. T_{rad} is shown only for $S_H = 0$ for more clear view. *Lower panels:* the line residual intensity profiles $R = I_\lambda/I^{cont}_\lambda$ (normalized to continuum intensity). The observed profile from the FTS atlas *(open circles)* is given for comparison. *All solid curves:* LTE. *All dotted, dashed, and dash-dotted curves:* non-LTE for $S_H = 0$, 0.1, and 1, respectively. The line formation heights in LTE *(vertical arrows)* and non-LTE *(filled circles)* are marked on the corresponding curves. $\log gf = 0.239$.

The underpopulation of the lower atomic level in the upper layers of the HOLMUL model occurs because there the ionizing UV radiation in continuum becomes hotter than the surrounding atmosphere, i. e., the excitation temperature T_{exc} of the UV radiation appreciably exceeds the electron temperature T_e. In the chromospheric layers of the MACKKL model the reverse happens ($T_{exc} < T_e$), therefore β_l increases with height.

At the same time, the upper level is underpopulated above 300 km in the model without chromosphere and overpopulated only above 800 km if there is the chromosphere in the model.

As can be seen in Fig. 1(a, b), the departure coefficient of the upper level β_u is sensitive to inelastic collisions with hydrogen atoms, while for the lower level this effect is small.

Figure 2(a, b) illustrates that the non-LTE effects in the granular and intergranular models are more or less similar to those obtained for the HOLMUL model. An exception is the larger β_l coefficient in the integranular model. Such an overpopulation is due to the weaker UV overionization in this model as compared with the granular one. Like in the HOLMUL model, in the 3D model the populations of both levels are close to LTE below 300 km. Above this height a drop of β_u occures with increasing height.

B. Line opacity

The non-LTE deviation of population of the lower atomic level causes a change of the line opacity. The non-LTE line opacity $\chi^{\rm L}$(NLTE) can be estimated from the LTE value $\chi^{\rm L}(LTE)$ by neglecting the stimulated emission processes: $\chi^{\rm L}$(NLTE) $\approx \beta_l \chi^{\rm L}$(LTE).

As can be seen in Fig. 1(a, b) and Fig. 2(b), the lower level of this line in the line formation layers of the HOLMUL, MACKKL, and integranular models is slightly overpopulated, while in the granular model this level is slightly underpopulated (see Fig. 2(a)). In all these models β_l is rather close to unity, therefore the scaling of the line opacity with this coefficient is unlikely to lead to any appreciable difference between the LTE and non-LTE formation heights of the line.

Table 2 confirms this conclusion. The shift of the line formation height caused by the non-LTE effects depends on the model atmosphere and $S_{\rm H}$. It ranges from −6 km in the granular model to 30 km in the MACKKL model. Figure 3 shows that in the 3D model such a shift is insignificant in comparison with spatial variations of the formation height. On average, in the 3D model the line is formed in non-LTE by 10 km higher than in LTE. In general, the core of the line is formed considerably deeper in granules than in intergranules, while for the line continuum the opposite effect takes place.

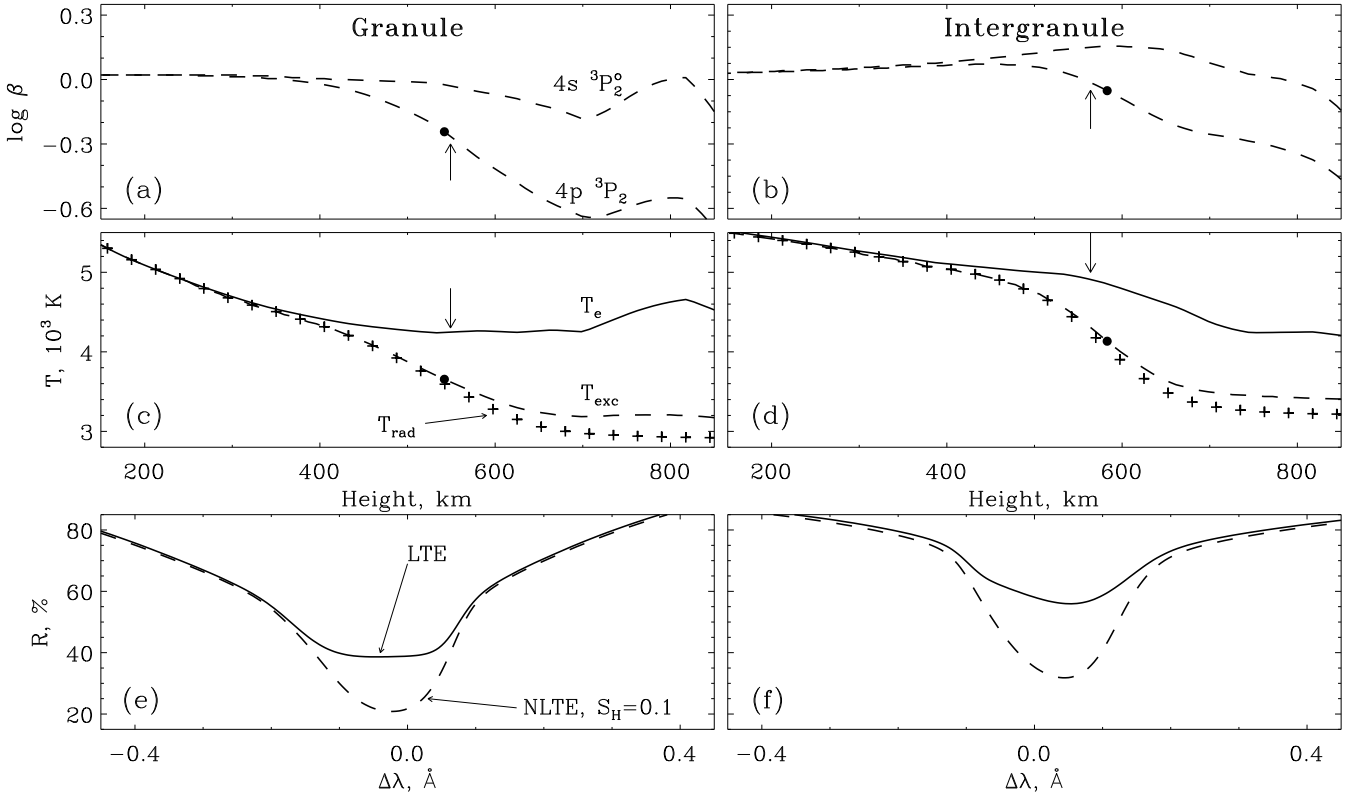

Fig. 2. Formation of the Si I 1082.7 nm line in the granular *(left panels)* and intergranular *(right panels)* models under LTE and non-LTE conditions. All notations are similar to those of Fig. 1. Only the non-LTE values for $S_{\rm H} = 0.1$ are shown in the figure for the sake of clarity.

Note an interesting side result: both the formation height and its shift are minimal in the VAL-C model, which has the smallest temperature and the highest temperature gradient at the line formation layers among the three 1D models.

C. Line source function

Figure 1(c, d) demonstrates the height dependence of the line source function $S^{\rm L}_\lambda$ calculated at line center in the units of excitation temperature $T_{\rm exc}$ for the 1D models HOLMUL and MACKKL. The $S^{\rm L}_\lambda$ values for the granular and intergranular models are shown in Figure 2(c, d). For comparison, there are also shown the Plank function B_λ and the mean intensity $\bar{J}_\lambda$ in the units of the corresponding temperatures.

The behavior of the Si I 1082.7 nm line source function follows the Wien approximation. According to it the β_u/β_l ratio sets the departure of the line source function from the Planck function $S^{\rm L}_\lambda(T_{\rm exc}) \approx \beta_u/\beta_l \cdot B_\lambda(T_{\rm e})$. As can be seen in Figs. 1(a, b) and 2(a, b), in all atmospheric models under consideration $\beta_u < \beta_l$ in the atmospheric layers above 300 km. Then $S^{\rm L}_\lambda < B_\lambda$, or, in temperature units, $T_{\rm exc} < T_{\rm e}$.

Note, that due to the shift of the line formation height

the deficit of $S_\lambda^{\rm L}$ becomes slightly larger in all models with the exception of the granular one. Such a deficit is sensitive to uncertainties in the inelastic collisions with hydrogen atoms. Figure 1(c, d) shows that the divergence between β_l and β_u decreases with increasing $S_{\rm H}$. As a result, the deviation of $S_\lambda^{\rm L}$ from B_λ becomes smaller.

Interestingly, in the formation height regions of the line $S_\lambda^{\rm L} \approx \bar{J}_\lambda$. This means that the line source function can be described sufficiently well using a two-level approximation.

Finally, we conclude that the source function deficit as compared with the LTE assumption is the main mechanism that control the formation of the Si I 1082.7 nm line. The line opacity shift is small and, hence, unimportant. On average, the non-LTE effects deepen the line profile.

	LTE	non-LTE			continuum
		$S_{\rm H}=0$	$S_{\rm H}=0.1$	$S_{\rm H}=1$	
HOLMUL	531	547	556	557	13
MACKKL	491	509	518	521	12
VAL-C	475	486	492	496	11
granule	547	—	541	—	30
intergranule	565	—	583	—	−61
3D (mean)	540 ± 30	—	550 ± 30	—	-30 ± 40

Table 2. Formation heights (in km) for the Si I 1082.7 nm line center and continuum under LTE and non-LTE conditions.

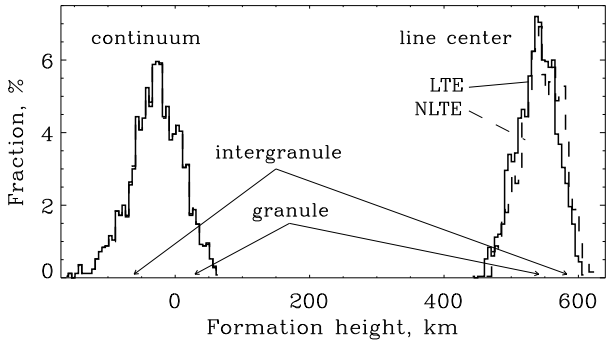

Fig. 3. Distribution of the formation height for the line center and continuum under LTE and non-LTE conditions in the 3D model. The arrows point the corresponding non-LTE heights in the granular and intergranular models. The bin size is 5 km.

D. Line profiles

Figure 1(e, f) shows the intensity profiles of the Si I 1082.7 nm line corresponding to the solar disk center for the models of HOLMUL and MACKKL. The profiles for the granular and intergranular models are shown in Fig. 2(e, f). The spatially averaged profiles for the 3D model are shown in Fig. 4. They all are computed for $\Omega = 1$, $A_{\rm Si} = 7.55$, $\log gf = 0.239$, $V_{\rm ma} = 1.85\,{\rm km\,s^{-1}}$ (for the 1D models only), and for different $S_{\rm H} = 0,\ 0.1,\ 1$. Everywhere in this text the line profiles represent the line intensity I_λ normalized to the continuum intensity $I_\lambda^{\rm cont}$, i.e., $R = I_\lambda / I_\lambda^{\rm cont}$ (hereinafter R is the residual intensity).

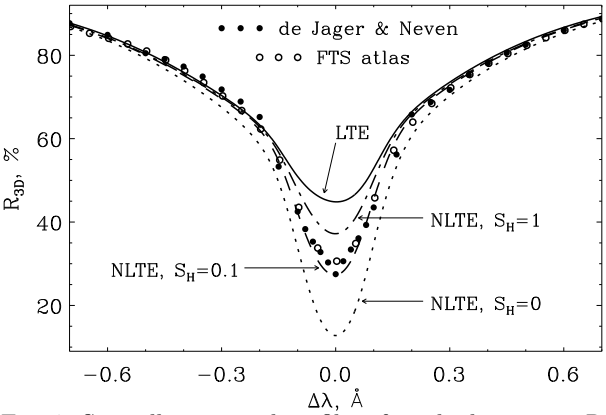

Fig. 4. Spatially-averaged profiles of residual intensity $R_{\rm 3D}$ of the Si I 1082.7 nm line computed in the 3D model under LTE and non-LTE conditions. The two observed profiles *(circles)* are given for comparison. The profiles are calculated for $\log gf = 0.239$.

As seen in these figures, the line source function deficit, indeed, deepens the theoretical non-LTE profiles in comparison with the LTE ones. Such a deficit is sensitive to $S_{\rm H}$, therefore the size of deepening strongly depends on $S_{\rm H}$. Figure 1(e, f) shows that the difference between the non-LTE and LTE line core residual intensity can reach 23% if we neglect collisions with hydrogen atoms ($S_{\rm H} = 0$).

The comparison of (e) and (f) panels of Fig. 2 makes clear that the line core depth depends also on the temperature gradient of the model atmosphere in the line formation region. The gradient is larger in granules, therefore the granular profile looks deeper than the intergranular one both in LTE and non-LTE. The flatter LTE line core is produced by a flatter height dependence of the electron temperature $T_{\rm e}$ in comparison with the steep height dependence of the excitation temperature $T_{\rm exc}$ (see Fig. 2(c, d)). Besides, due to the convective motions the line core is blueshifted in the granular model and redshifted in the intergranular one.

All these results confirm the conclusions made earlier by Bard & Carlsson [31] and Shi et al. [30]: LTE is a poor approximation for this line. Under the non-LTE conditions, the computations cannot reproduce the observed line core, if inelastic collisions with hydrogen are not included ($S_{\rm H} = 0$). The line core is too deep due to strong non-LTE effects caused by the line source function deficit. In the 3D model the line core is even deeper than in the 1D models. The only possibility to reproduce observations is to take into account inelastic collisions with hydrogen atoms. Figure 1(e, f) shows that in the 1D models the best-fit to the observed profile can be obtained with $S_{\rm H} = 1$, while in the 3D model—for $S_{\rm H} \approx 0.1$.

The larger value of $S_{\rm H}$ in the 1D models could be attributed to the masking effect because such models cannot reproduce real atmospheric inhomogeneities. We will quantify this conclusion in the next section.

IV. UNCERTAINTIES

The modeling of line profiles usually involves many input parameters. The most important of them: model atmospheres, rates of collisions with electrons, rates of inelastic collisions with hydrogen atoms, line oscillator strength, macroturbulent velocity (for 1D models only). In this section we test the sensitivity of the Si I 1082.7. nm line profile to the above parameters.

A. Choice of model atmosphere

Upper panel of Fig. 5 shows how the non-LTE residual intensity R changes when we use different 1D model atmospheres. The absolute change of R varies only within 1.5% if the MACKKL or the VAL-C models are chosen instead of the HOLMUL. This effect is smaller for the higher values of Ω and $S_{\rm H}$. This means that in the 1D case the effect of model selection on the resulting profile is small.

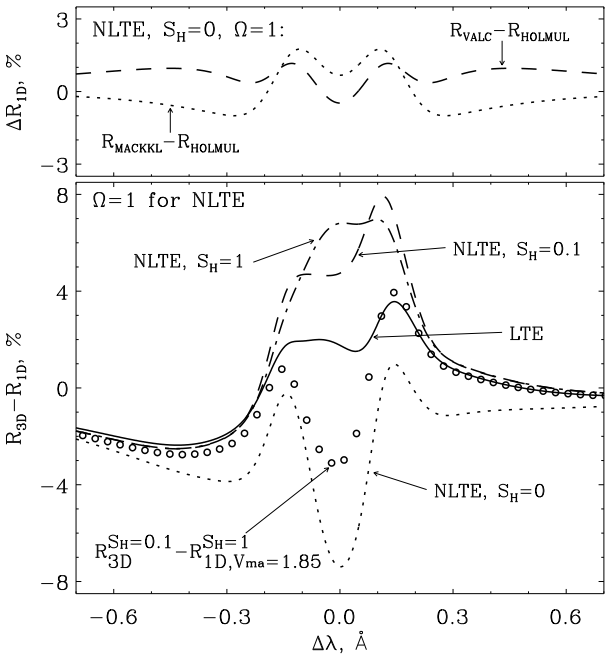

Fig. 5. Changes of the line residual intensity ΔR caused by using different model atmospheres. *Top panel:* results for the 1D semi-empirical models. *Bottom panel:* changes ΔR caused by using the 3D model instead of the 1D HOLMUL model. *Open circles:* the difference between the line residual intensity calculated in the 3D model for $S_{\rm H} = 0.1$ and the residual intensity calculated in the HOLMUL model for $S_{\rm H} = 1$. $\log gf = 0.239$.

The bottom panel of Fig. 5 demonstrates the effects produced by the 3D model topology. The differences ΔR are calculated for different $S_{\rm H}$. The rest of the parameters are fixed.

There are several effects of atmospheric inhomogeneities, or, in other words, "3D effects".

First, all $R_{\rm 3D}$ profiles are asymmetrical. The far blue wing of the $R_{\rm 3D}$ profile is more than 2% deep as compared with the $R_{\rm 1D}$ profile both in LTE and non-LTE. The change of the far red wing of the profile is small.

Secondly, the line core becomes shallower by 2–3% due to the broadening by the convective motions and the differences in the temperature structure between 1D and 3D models, as it follows from the LTE profile. Joint action of the non-LTE and 3D effects rises the line core by 5–8%, as it follows from the non-LTE profile for $S_{\rm H} > 0$. If there are no collisions with hydrogen atoms ($S_{\rm H} = 0$), the line core in the 3D model turns out to be deeper by 8% relatively to the 1D case.

The results shown by circles in the bottom panel of Fig. 5 confirm our assumption made in the previous section. As seen in this figure, the difference between the best-fit line profiles calculated using the 3D and the HOLMUL models is relatively small. This means that an order of magnitude difference between the best-fit $S_{\rm H}$ in the 1D and 3D models can be attributed to the effects of atmospheric inhomogeneities.

B. Uncertainties of collisional rates

We tested how the uncertainties of the collisional rates with electrons and the inelastic collisional rates with hydrogen atoms affect the non-LTE modeling of the Si I 1082.7 nm line. For this aim we compared the line profiles calculated for different collisional strengths $\Omega = 1$, 10 and for different scaling factors $S_{\rm H} = 0$, 0.1, 1.

The resulting profiles were subtracted for the observed profile to see which set of the parameters reproduces the observations in the best way.

The results of such a comparison for the 1D and 3D models are shown in Fig. 6.

It is impossible to reproduce the observed line core in the 1D model if $S_{\rm H} = 0$ even for $\Omega = 10$. For $V_{\rm ma} = 1.85\,{\rm km\,s^{-1}}$ the best fit to observations is obtained for $S_{\rm H} = 1$ and $\Omega = 1$. In this case, using of $\Omega = 10$ does not make any considerable improvement. An order of magnitude increase of Ω increases the line core intensity by less than 3.5% if $S_{\rm H}$ is fixed. Similar results are obtained for the models of MACKKL and VAL-C. In the VAL-C model the best-fit $S_{\rm H}$ is a little bit higher than 1. This may be caused by different temperatures in the temperature minimum, rather than by the chromospheric rise of the temperature.

In the 3D model the best fit is reached for $S_{\rm H} = 0.1$ and $\Omega = 1$. A little worse fit can be reached for $S_{\rm H} = 0$ and $\Omega = 10$. However, the latter value gives a strong overestimation of the most collisional rates [63]. Note that in the 3D model the collisional effects are much stronger. With an increase of Ω by an order of magnitude the line core R increases by 13%, 10% and 7% for $S_{\rm H} = 0$, 0.1 and 1, respectively. Almost the same happens if $S_{\rm H}$ increases while Ω is fixed.

We finally conclude that in order to reproduce the observations of the Si I 1082.7 nm line we have to take into account inelastic collisions with hydrogen atoms both in the 1D and 3D models.

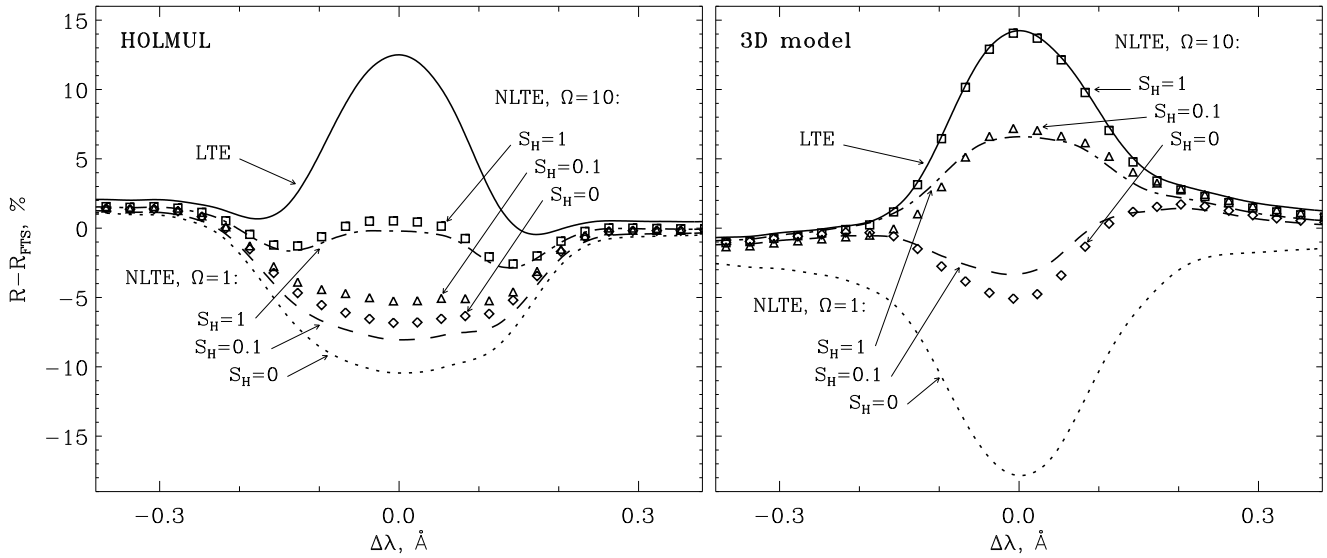

Fig. 6. Differences between the calculated R and observed $R_{\rm FTS}$ residual intensity profiles of the Si I 1082.7 nm line in the HOLMUL *(left panel)* and the 3D *(right panel)* models. R are computed for LTE and for non-LTE with different values of Ω and $S_{\rm H}$. $R_{\rm FTS}$ is taken from the FTS atlas. $\log gf = 0.239$.

C. Combined effects of uncertainties of $S_{\rm H}$, $\log gf$, and $V_{\rm ma}$

We investigated the sensitivity of the line profile to the combined effect of uncertainties in the scaling factor $S_{\rm H}$, the line oscillator strength $\log gf$, and the macroturbulent velocity $V_{\rm ma}$ (for 1D models) in order to determine these values more accurately.

The line parameters, which we have chosen for the analysis, are the line central depth D, the equivalent width W and the profile width L_{80}. The latter parameter represent the full width of the line profile between two points where $R = 80\%$. We prefer this parameter instead of the widely used full width at a half maximum (FWHM) for the following reasons.

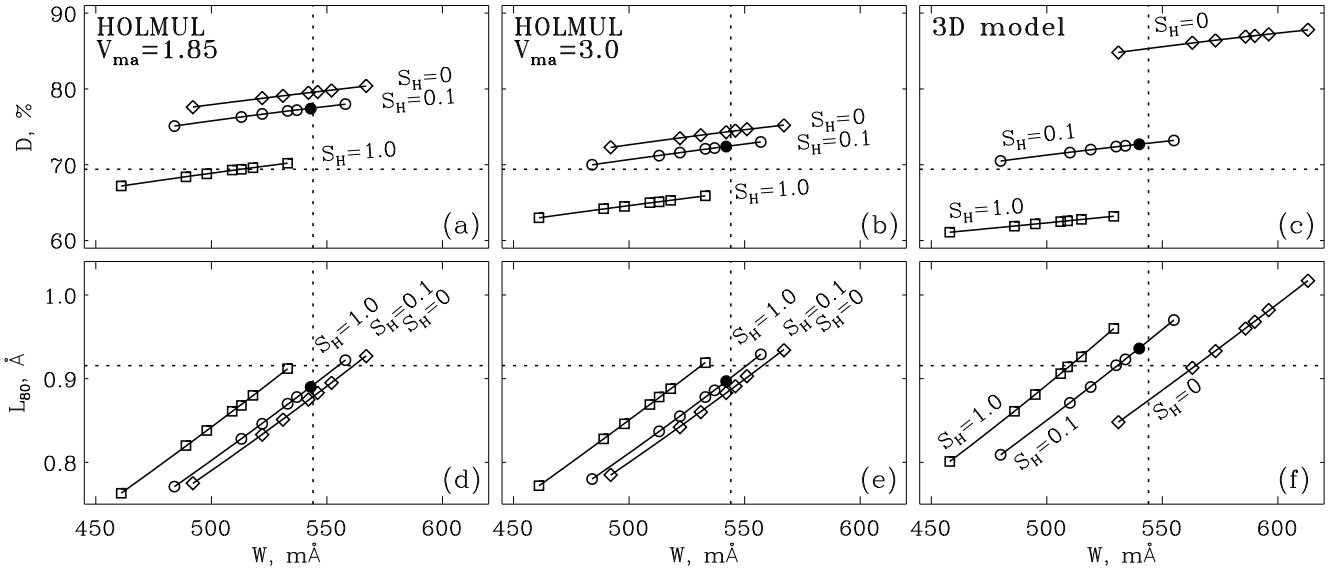

Fig. 7. Dependencies between the central depth D, the profile width L_{80}, and the equiwalent width W of the Si I 1082.7 nm line under non-LTE conditions in the HOLMUL and the 3D models. *Left and middle panels:* results in the HOLMUL model for $V_{\rm ma} = 1.85$ and $3\,{\rm km\,s^{-1}}$, respectively. *Right panels:* results in the 3D model. Solid lines connect the groups of parameters computed for fixed $S_{\rm H}$, but for different $\log gf$ (see Table 1). D, L_{80}, and W increase with increasing $\log gf$. Filled circles indicate the parameters computed for $\log gf = 0.239$ of Froese-Fischer and $S_{\rm H} = 0.1$. Dotted lines show the observed parameters of the FTS atlas profile.

The FWHM corresponds to the profile points where the line core turns into wings. The core of such strong lines tends to be saturated, and the equivalent width of such profile is mainly sensitive to the line wing broadening. Therefore, the FWHM weakly depends on W. In contrast to FWHM, the L_{80} parameter is sensitive enough to wing broadening because we measure it close to the line continuum. Besides, in this part of the line profile there are no blends.

We compared the computed D, W, and L_{80} values with the observed ones, measured from the FTS atlas profile. The measurement errors are less than 1% for D and L_{80}, and are about 5% for W.

We computed the parameters in non-LTE for the selected set of $\log gf$ values (see Table 1) and for different $S_{\rm H}$. In the 1D model we used two values of $V_{\rm ma} = 1.85$ and $3\,{\rm km\,s^{-1}}$. The results for the HOLMUL model are shown in Fig. 7(a, b, d, e). The results for the 3D model are shown in Fig. 7(c, f).

As can be seen from the figure, L_{80} is more sensitive to $\log gf$ than D. On the other hand, D is more sensitive to $S_{\rm H}$ than L_{80}. In addition, in the 1D models D significantly depends on $V_{\rm ma}$, while L_{80} is not.

Such a behavior of $D(W)$ and $L_{80}(W)$ dependencies makes it possible to estimate the best values of $S_{\rm H}$ and $\log gf$ by fitting the computed D and L_{80} values to the observed ones.

In the 1D case we get $S_{\rm H} = 1$ and $\log gf = 0.273$ for $V_{\rm ma} = 1.85\,{\rm km\,s^{-1}}$. If $V_{\rm ma} = 3\,{\rm km\,s^{-1}}$ then an order of magnitude smaller $S_{\rm H}$ is needed, while $\log gf$ does not change. Our estimates of the best-fit $S_{\rm H}$ obtained with different values of $V_{\rm ma}$ explain why Shi et al. [30] got the lower value of $S_{\rm H} = 0.1$ from the 1D modeling. In contrary to us, Shi et al. fitted the line flux profiles. The flux is calculated by integrating the intensity over the solar disk. Therefore the value of $V_{\rm ma}$ used by these authors has to be higher than that needed to fit the solar disk center intensity. As a result, their value of $S_{\rm H}$ is smaller.

Figure 7(c, f) shows that in comparison with the 1D case, in the 3D models the dependence of D and L_{80} on $S_{\rm H}$ is much stronger. Therefore, we can get more reliable estimates. In the 3D case the best-fit values are $\log gf \approx 0.24$ and $S_{\rm H} \approx 0.1$ (even a little bit larger). We recommend these values for further modeling of the Si I 1082.7 nm line.

DISCUSSION AND CONCLUSIONS

We investigated the formation of the Si I 1082.7 nm line under non-LTE using different 1D models of the solar atmosphere. There are two main non-LTE effects that control the formation of this line. They are the line opacity change and the line source function deficit. The first effect causes a small shift of the line formation height in the range from -6 to 30 km. As a result, it has almost no influence on the line profile. The second effect is more intense, it significantly decreases the line core intensity. Our results of the non-LTE modeling of the Si I 1082.7 nm line in the 1D models agree well with the results of Bard & Carlsson [31].

We also investigated the formation of this line under non-LTE in the 3D HD model of the solar atmosphere neglecting the effects of a horizontal radiative transfer. Like in the 1D case, we found significant LTE vs. non-LTE discrepancies and similar non-LTE effects. The size of these effects depends on the thermodynamic structure of the granules and the intergranules being larger in the intergranules. Contrary to expectations of Bard & Carlsson, we found that under non-LTE the line core intensity of the spatially-averaged profile in the 3D model is lower than that in the 1D case if we neglect inelastic collisions with hydrogen atoms.

In order to fit the synthetic and observed line profiles, and to compensate for strong non-LTE effects in the line core, we introduced inelastic collisions with the hydrogen atoms. For this aim we used the Drawin formula. We keep in mind that this formula can be far from reality (see the review by Barklem *et al.* [64]). There is no reliable cross-sections for Si + H collisions, so we applied the empirical scaling factor $S_{\rm H}$ for this formula. In the 1D models, our best-fit value is $S_{\rm H} = 1$, which contradicts the lower value $S_{\rm H} = 0.1$ of Shi et al. [30]. However, in the 3D model, our best-fit estimate is $S_{\rm H} = 0.1$. Such a difference may be caused by using a larger value of macroturbulent velocity needed to fit the flux profile as it takes places in the paper of Shi et al.

3D models make it possible to avoid the masking of real inhomogeneities of the solar atmosphere, hidden in the larger value of $S_{\rm H} = 1$ as it occures in the 1D case. However, the smaller value $S_{\rm H} \approx 0.1$ found from the non-LTE modeling of the Si I 1082.7 nm line in the 3D model cannot be considered as a final value. It has to be even smaller if other effects, hidden in the best-fit $S_{\rm H}$, are properly accounted for. We may only speculate what these effects are. They might be either the inaccuracies of inelastic collisions with electrons, or charge exchange reactions like $Si^* + H \leftrightarrow Si^+ + H^-$ (see Fig. 6 in [65]), which are usually stronger for infrared lines. Such effects could not be verified now due to lack of precise experimental data. Another effect not considered here is the line broadening caused by small-scale magnetic fields of the quiet solar atmosphere. We shall study this effect in our next paper.

Therefore, we recommend the following best-fit values for further modeling of the Si I 1082.7 line transition: $\log gf \approx 0.24$, and $S_{\rm H} \approx 0.1$. The latter value should be taken with care.

ACKNOWLEDGMENTS

The author is grateful to his supervisor Nataliya Shchukina for the support and discussions, and to Vyacheslav Olshevsky for useful comments on the manuscript. This research was supported by two grants number 0111U004495 (GEOCOSMOS) and 010U002124 of the NAS of Ukraine.

[1] A. Lagg, Adv. Space Res. **39**, 1734 (2007).
[2] S. A. Chuprakov *et al.*, in *Multi-Wavelength Investigations of Solar Activity*, edited by A. V. Stepanov, E. E. Benevolenskaya, A. G. Kosovichev, IAU Symp. **223**, 183 (2004).
[3] T. A. Schad *et al.*, in *Solar Polarization 6*, edited by J. R. Kuhn *et al.*, ASP Conf. Ser. **437**, 483 (2011).
[4] K. Muglach *et al.*, Adv. Space Res. **25**, 1731 (2000).
[5] D. Orozco Suarez, A. Lagg, S. K. Solanki, in *ESA SP-596*, edited by D. E. Innes, A. Lagg, S. K. Solanki, ESA SP Publ. **596**, 59 (2005).
[6] R. Centeno, M. Collados, J. Trujillo Bueno, in *Solar Polarization 4*, edited by R. Casini, B. W. Lites, ASP Conf. Ser. **358**, 465 (2006).
[7] H. Lin, M. J. Penn, J. R. Kuhn, Astrophys. J. **493**, 978 (1998).
[8] Xu Z. *et al.* Astrophys. J. **749**, 138 (2012).
[9] L. Yelles Chaouche *et al.* Astrophys. J. **748**, 23 (2012).
[10] S. Solanki *et al.*, Nature **425**, 692 (2003).
[11] T. Wiegelmann *et al.*, Astron. Astrophys. **433**, 701 (2005).
[12] M. J. Penn, J. R. Kuhn, Astrophys. J. **441**, L51 (1995).
[13] `http://solar-b.nao.ac.jp/SOLAR-C/index_e.html`
[14] R. Centeno, M. Collados, J. Trujillo Bueno, Astrophys. J. **640**, 1153 (2006).
[15] R. Centeno, M. Collados, J. Trujillo Bueno, Astrophys. J. **692**, 1211 (2009).
[16] T. Felipe *et al.*, Astrophys. J. **722**, 131 (2010).
[17] T. Felipe *et al.*, J. Phys. Conf. Ser. **271**, 012040 (2011).
[18] T. Felipe, E. Khomenko, M. Collados, Astrophys. J. **735**, id65 (2011).
[19] J. Hofmann, F.-L. Deubner, B. Fleck, in *GONG'94: Helio- and Astro-Seismology*, edited by R. K. Ulrich, E. J. Rhodes, Jr., W. Däppen, ASP Conf. Ser. **76**, 342 (1995).
[20] D. Sh. Bloomfield, A. Lagg, S. K. Solanki, Astrophys. J. **671**, 1005 (2007).
[21] D. Sh. Bloomfield *et al.*, in *The Physics of Chromospheric Plasmas*, eds. P. Heinzel, I. Dorotovič, R. J. Rutten, ASP Conf. Ser. **368**, 239 (2007).
[22] M. J. Penn, C. L. Allen, Solar Phys. **174**, 359 (1997).
[23] W. Livingston, H. Holweger, Astrophys. J. **252**, 375 (1982).
[24] A. K. Pierce, J. C. Lopresto, Solar Phys. **93**, 155 (1984).
[25] Ж. А. Пожалова, Письма Астрон. Журн. **13**, 610 (1987).
[26] Ж. А. Пожалова, Астрон. Журн. **65**, 1037 (1988).
[27] R. Centeno *et al.*, Astrophys. J. **677**, 742 (2008).
[28] J. Trujillo Bueno *et al.*, Nature **415**, 403 (2002).
[29] J. Trujillo Bueno, A. Asensio Ramos, Astrophys. J. **655**, 642 (2007).
[30] J. R. Shi *et al.*, Astron. Astrophys. **486**, 303 (2008).
[31] S. Bard, M. Carlsson, Astrophys. J. **682**, 1376 (2008).
[32] A. V. Sukhorukov, N. G. Shchukina, Kinem. Phys. Celest. Bodies **28**(1), 27 (2012).
[33] A. V. Sukhorukov, N. G. Shchukina, Kinem. Phys. Celest. Bodies **28**(4), 169 (2012).
[34] H. W. Drawin, Z. Phys. **211**, 404 (1968).
[35] H. W. Drawin, Z. Phys. **225**, 483 (1969).
[36] L. Golbderg, E. A. Müller, L. H. Aller, Astrophys. J. Suppl. Ser. **5**, 1 (1960).
[37] W. van Rensbergen, Solar Phys. **11**, 11 (1970).
[38] B. Warner, Mon. Notic. Roy. Astron. Soc. **139**, 1 (1968).
[39] R. L. Kurucz, E. A. Peytremann, *A table of semiempirical gf values. Part 1: Wavelengths: 5.2682 nm to 272.3380 nm* (SAO Special Report, Cambridge, Mass., 1975).
[40] C. Froese Fischer, Phys. Rev. A. **71**, 042506 (2005).
[41] J. M. Borrero *et al.*, Astron. Astrophys. **404**, 749 (2003).
[42] `http://www.nist.gov/pml/data/asd.cfm`, v. 4
[43] S. D. Anstee, B. J. O'Mara, Mon. Notic. Roy. Astron. Soc. **253**, 549 (1991).
[44] S. D. Anstee, B. J. O'Mara, Mon. Notic. Roy. Astron. Soc. **276**, 859 (1995).
[45] P. S. Barklem, B. J. O'Mara, Mon. Notic. Roy. Astron. Soc. **290**, 102 (1997).
[46] P. S. Barklem, B. J. O'Mara, J. E. Ross, Mon. Notic. Roy. Astron. Soc. **296**, 1057 (1998).
[47] Э. А. Гуртовенко, Р. И. Костык, *Фраунгоферов спектр и система солнечных сил осцилляторов* (Наук. Думка, Киев, 1989).
[48] E. Anders, N. Grevesse, Geochim. Cosmochim. Acta **53**, 197, (1989).
[49] N. Shchukina, A. Sukhorukov, J. Trujillo Bueno, Astrophys. J. **755**, 176 (2012).
[50] M. Asplund, Ann. Rev. Astron. Astrophys. **43**, 481 (2005).
[51] N. G. Shchukina, A. V. Sukhorukov, Kinem. Phys. Celest. Bodies **28**(2), 49 (2012).
[52] H. Holweger, E. A. Müller, Solar Phys. **39**, 19 (1974).
[53] P. Maltby *et al.*, Astrophys. J. **306**, 284 (1986).
[54] J. E. Vernazza, E. H. Avrett, R. Loeser, Astrophys. J. Suppl. Ser. **45**, 635 (1981).
[55] M. Asplund *et al.*, Astron. Astrophys. **359**, 669 (2000).
[56] N. Shchukina, J. Trujillo Bueno, Astrophys. J. **550**, 970 (2001).
[57] M. Asplund *et al.*, Astron. Astrophys. **359**, 729 (2000).
[58] O. Espagnet *et al.*, Astron. Astrophys. Suppl. Ser. **109**, 79 (1995).
[59] Р. И. Костык, Н. Г. Щукина, Астрон. Журн. **81**, 846 (2004).
[60] H. Neckel, D. Labs, Solar Phys. **90**, 205 (1984).
[61] H. Neckel, Solar Phys. **184**, 421 (1999).
[62] C. de Jager, L. Neven, Bull. Astr. Inst. Netherlands Suppl. **1**, 325 (1967).
[63] C. W. Allen *Astrophysical quantities* (Athlone Press, London, 1973)
[64] P. S. Barklem *et al.*, Astron. Astrophys. **530**, A94 (2011).
[65] K. Lind *et al.*, Astron. Astrophys. **528**, A103 (2011).

НЛТР ФОРМУВАННЯ ЛІНІЇ SI I 1082.7 нм В ОДНО- ТА ТРИВИМІРНИХ МОДЕЛЯХ СОНЯЧНОЇ АТМОСФЕРИ

А. В. Сухоруков
Головна астрономічна обсерваторія НАН України,
вул. Академіка Заболотного, 27, Київ, 03680, Україна

Досліджено формування лінії Si I 1082.7 нм в різних одновимірних (1D) напівемпіричних та тривимірній гідродинамічній (3D ГД) моделях атмосфери Сонця. Знайдено значні відхилення від ЛТР в усіх моделях. Вони викликані зсувом висоти формування лінії та дефіцитом функції джерела лінії. В 3D-моделі інтенсивність у ядрі лінії при НЛТР набагато нижча, ніж у 1D-моделях, якщо знехтувати непружними зіткненнями з атомами водню. Можна компенсувати сильні НЛТР-ефекти й отримати узгодження зі спостережннями для 3D-моделі, якщо скористатися для опису таких зіткнень формулою Дроіна з множником $S_{\rm H} = 0.1$. В 1D-моделях, що не описують реальних неоднорідностей атмосфери, узгодження отримано для більшого значення $S_{\rm H} = 1$. Оцінено силу осцилятора $\log gf$ цієї лінії. Вона становить близько 0.27 для 1D-моделей та 0.24 для 3D-моделі.